

Molecular dynamics study of ethanol solvated by water on the Pt (1 1 1) surface

Kholmirzo Kholmurodov^{a,b,*}, Ermuhammad Dushanov^{a,c}, Kenji Yasuoka^d, Hagar Khalil^e, Ahmed Galal^e, Sameh Ahmed^f, Nasser Sweilam^f, Hatem Moharram^f

^a Laboratory of Radiation Biology, Joint Institute for Nuclear Research, Dubna, Moscow Region, Russia

^b Dubna International University, Dubna, Moscow Region, Russia

^c Institute of Nuclear Physics, Tashkent, Uzbekistan

^d Department of Mechanical Engineering, Keio University, Japan

^e Chemistry Department, Faculty of Science, Cairo University, Egypt

^f Mathematics Department, Faculty of Science, Cairo University, Egypt

ARTICLE INFO

Article history:

Received 2 November 2011

In final form 3 April 2012

Available online 23 April 2012

Keywords:

Molecular dynamics simulations

Ethanol molecule

Water active solvent

Diffusion coefficient

Pt surface

ABSTRACT

An analysis of the molecular dynamics of ethanol solvated by water molecules in the absence and presence of the Pt (1 1 1) surface has been performed using DL_POLY version 2.19. The structure and diffusion properties of an ethanol–water system have been studied at various temperatures from 250 to 350 K. We have measured the self-diffusion coefficients of a 50:50% ethanol–water system; in the absence of a Pt surface our results have shown an excellent agreement with the experimental data (within an error of 7.4%). The enhancement of self-diffusion coefficients with the inclusion of the Pt (1 1 1) surface has been observed and estimated. Graphs of radial distribution functions (RDF) have been built; RDF correlations with the self-diffusion coefficients of both ethanol and water molecules are also illustrated.

© 2012 Elsevier B.V. All rights reserved.

1. Introduction

In recent years, there has been a great interest in studying the chemical and physical properties of ethanol on a Pt surface, as ethanol is one of the most important renewable fuels [1]. The intensive utilization of fossil fuels has led to an increase in the generation of polluting gases released into the atmosphere, which has caused changes in the global climate. The solution to this problematic issue depends on how the development and implementation of technologies based on alternative sources of energy will be undertaken. Among the renewable energy resources, ethanol (ethyl alcohol, bio-ethanol) is the most practical liquid biofuel – both as a fuel and a gasoline enhancer. It is not toxic, does not contaminate water sources [2], and can be produced in large quantities from agricultural products or biomass, which will not change the natural balance of carbon dioxide in the atmosphere in contrast to the use of fossil fuels [3].

Ethanol has been considered in recent years, and it has a lot of applications. The most popular application is fuels because of a decrease in the available petroleum resources. For ethanol to be a

fuel, the water content in ethanol should be less than 1.3% [4], which is hard to reach by crystallization. Pervaporation separation is a valuable method that can save money, and therefore much research is focused on it. Direct ethanol fuel cells (DEFCs) are another important application for the conversion of chemical energy to electricity [5,6]. Water and ethanol can be used not only in fuels, but also in other applications, such as being a solvent to accelerate the aging of some polymeric materials [7] and being used in commercial cooling systems because of their good thermophysical and technological characteristics [8]. An alcohol–water mixture often shows quite different properties than the corresponding pure components. Of particular interest are the structure and diffusion properties, which play important roles in the theoretical study and technological applications involving mass transfer [9]. In addition, from a microscopic viewpoint, the knowledge of solution structure behavior is very fundamental to understanding and elucidating the mixture diffusion phenomenon.

Molecular dynamics simulation is a powerful tool in investigating the structure properties of solutions at the molecular level, and it has been widely used to study aqueous solutions [10,11]. Metal surfaces are often used in the synthesis of oxygen containing compounds, such as alcohols, and in the degradation of these oxygen-containing compounds, where carbon–carbon (C–C) and carbon–oxygen (C–O) bond formation and breakage are the elementary steps in this type of process, and the metal surface plays a primary role in the efficiency and selectivity of these steps

* Corresponding author at: Laboratory of Radiation Biology, Joint Institute for Nuclear Research, Dubna, Moscow Region, Russia.

E-mail addresses: mirzo@jinr.ru (K. Kholmurodov), eric.dushanov@gmail.com (E. Dushanov), yasuoka@mech.keio.ac.jp (K. Yasuoka), hagar@sci.cu.edu.eg (H. Khalil), galal@sci.cu.edu.eg (A. Galal), sameh.ahmed@sci.cu.edu.eg (S. Ahmed), nsweilam@sci.cu.edu.eg (N. Sweilam), hatem@sci.cu.edu.eg (H. Moharram).

[12]. Platinum is the most known catalyst for the oxidation of such molecule. It is known to activate the dissociative adsorption of ethanol at an appreciable rate [13]. Thus, studying the adsorption of ethanol on a platinum surface can give more information on the kinetics of this process. Molecular dynamics (MD) simulation is one of the most important computational tools to study the liquid–surface interaction. At a high temporal resolution, MD processes may provide information on the dynamics of the system and the events which take place on the surface within a few picoseconds [14]. The application of molecular dynamics to liquids or solvent–solute systems allows the computation of properties such as diffusion coefficients or radial distribution functions for use in statistical mechanical treatments [15].

Few researches were performed on ethanol–water surface. C. Zhang and X. Yang studied the structure behavior and diffusion properties for an ethanol–water solution and investigated the concentration dependence of properties [9]. Wang Yao-Chun et al. used MD simulation to investigate the behavior of pure water molecules, ethanol molecules, and water–ethanol mixture with various weight fractions inside Au nanotubes [7]. Miyabe and Takeuchi estimated the surface diffusion coefficient in the liquid phase adsorption using a restricted diffusion model, where the diffusion coefficient is correlated with the molecular diffusivity by considering an energy restriction due to adsorptive interaction between adsorbates and adsorbents [16]. Cooke et al. studied the interface between the {10 $\bar{1}$ 4} surface of calcite and pure ethanol, pure water, and 50:50 mixture (by amount) of water and ethanol [17].

To the best of our knowledge, little is known from literature surveys about the interesting ethanol–water interactions in the presence of Pt surfaces. In the present work, using the MD method, we have simulated ethanol–water system in the absence and presence of a platinum surface through a wide temperature range – from 250 to 350 K – and calculated self-diffusion coefficients. The enhancement of the self-diffusion coefficients of both water and ethanol molecules correlating with the ethanol–water structure has been well established in the presence of a Pt surface.

2. Simulation method

We have studied the molecular dynamics of a water–ethanol solution system in the absence and presence of a platinum surface using the DL_POLY 2.19 code, which was developed by the Molecular Simulation Group at the Daresbury Laboratory (England) with the support of the Research Council for the Engineering and Physical Sciences (project CCP5 of the simulation of condensed phases). DL_POLY is a general-purpose MD simulation package developed by W. Smith, T.P. Forester and I.T. Todorov [18,19].

2.1. Simulation details

Ethanol and water molecules are described using the force field from the DL_POLY database [18,19], where bonding, angular, and dihedral parameters are incorporated into standard molecular mechanics potentials. All nonbonding interactions are accounted for via Lennard–Jones (LJ) potentials and Coulombic interactions based on the partial charges associated in each atom. For water, the SPC model is used. The computer simulations have been performed for a MD cell of a volume $V = (54.92, 54.92, 63.8) \text{ \AA}^3$ under the energy and temperature control at $T = 298 \text{ K}$ and other temperatures. Starting with a 50:50 (by molecules) water–ethanol solution, with a corresponding density of 0.78 g/cm^3 and 588 Pt₄ molecules of 2352 atoms, the total number of atoms in the system was $N = 16,176$; the chemical bonds are constrained within a flexible bond with a length of 1 Å. The integration of the equations of

motion was performed using the Verlet integration scheme in quaternion. The integration step was 1 fs (femtosecond); a microcanonical (nvt) ensemble was used for the simulated system, and the Nose–Hoover algorithm was employed to keep the desired temperature. The intermolecular chemical bonds were estimated on the basis of the Shake algorithm with an accuracy of 10^{-8} . The Ewald summation with a convergence parameter of 10^{-6} was used for the calculation of electrostatics forces in the periodic system [18,19]. The total number of steps was 100,000 for each temperature, and all simulations were periodic in three dimensions.

The configuration energy of the molecular model is represented as a sum of the energies of the bonding (E_{val}) and non-bonding (E_{nb}) interactions:

$$E = E_{\text{val}} + E_{\text{nb}} \quad (1)$$

The energy of the valence (bonding) interactions E_{val} is given by the following formula:

$$E_{\text{val}} = E_{\text{bond}} + E_{\text{ang}} + E_{\text{dih}} + E_{\text{teth}}, \quad (2)$$

where E_{bond} is the energy of chemical bonds, E_{ang} is the energy of angular bonds, E_{dih} is the energy of dihedral bonds, and E_{tether} is tether energy.

The energy of the non-valence (non-bonded) interactions is a sum of the energies of the van-der-Waals (vdW), electrostatics (Coulomb), and hydrogen bonds:

$$E_{\text{nb}} = E_{\text{vdW}} + E_{\text{coul}} \quad (3)$$

During the MD simulations, the following potential types, which represent the topology of the molecular field for an ethanol–water system, were used [19]:

$$\text{Harmonic bond potential : } U(r_{ij}) = \frac{1}{2}K(r_{ij} - r_0)^2 \quad (4)$$

$$\text{Harmonic bond angle : } U(\theta_{ijk}) = \frac{1}{2}K(\theta_{ijk} - \theta_0)^2 \quad (5)$$

$$\text{Harmonic dihedral : } U(\phi_{ijkn}) = \frac{1}{2}K(\phi_{ijkn} - \phi_0)^2 \quad (6)$$

$$\text{The Lennard–Jones potential : } U_{ij}(r_{ij}) = 4\varepsilon_{ij} \left[\left(\frac{\sigma_{ij}}{r_{ij}} \right)^{12} - \left(\frac{\sigma_{ij}}{r_{ij}} \right)^6 \right] \quad (7)$$

$$\text{Coulombic interaction : } U(r_{ij}) = \frac{1}{4\pi\varepsilon_0} \cdot \frac{q_i q_j}{r_{ij}} \quad (8)$$

$$\text{Quartic tether potential : } U(r_{ij}) = \frac{1}{2}kr_{ij}^2 + \frac{1}{2}kr_{ij}^4 \quad (9)$$

The tether potential suggests that the momentum will no longer be a conserved quantity of the simulation. The force on the atom “ i ” arising from the tether potential is obtained using the general formula:

$$\underline{F}_j = -\frac{1}{r_{io}} \left[\frac{\partial}{\partial r_{io}} U(r_{io}) \right] \underline{r}_{io} \quad (10)$$

where σ_{ij} is the size parameter, ε_{ij} the energy parameter, $\sigma_{ij} = (\sigma_i + \sigma_j)/2$ and $\varepsilon_{ij} = \sqrt{\varepsilon_i \varepsilon_j}$, q_i is the charge of site i and r_{ij} the distance between sites i and j . We choose the values of $k = 0.2$ and $k' = 0.4$ to avoid the destruction of our surface during heating and annealing processes.

Water was represented by the constrained OW–HW bond potential; thus a SPC model was used. Tables 1 and 2 contain bond lengths and intermolecular Lennard–Jones parameters for ethanol,

Table 1

Bond lengths in the ethanol molecules; for the water the OW–HW bond constrained on 1 Å.

Bond	K (kcal mol ⁻¹ Å ⁻²)	L (Å)
C ₁ –C ₂	222	1.52
C–H	309	1.11
C ₁ –Oe	428	1.42
Oe–He	545	0.94

water molecules, and a Pt surface respectively. An organic force field used to describe the ethanol molecules is presented in Table 3. As it was mentioned above for the organic force field in describing the ethanol molecule both dl-field and dl-poly data bases were employed as references, where the ethanol force field data are already fitted and tabulated in these data bases. Generally, the ethanol and organic force fields are also accessible from the CHARMM database. For more detailed information about the interaction potentials of the ethanol and other organic molecules we refer the readers to the CHARMM c36b1 Documentation [20,21]. The CHARMM force field parameters were derived from quantum mechanical calculations; it is worth noting that CHARMM was also ported to other force field formats and widely used by AMBER, GROMACS, and DL_POLY general-purpose MD simulation programs. These force fields reflect the most prominent improvements with the adjustment and reparameterization of charges, dihedral angle parameters, and so on [22–24]. In a great number of studies, the force fields have been shown to well reproduce the experimental values of hydration enthalpy, entropy, heat capacity, etc., and therefore they have been used for the adsorption of solutes from the bulk solutions to metal surfaces or aqueous environments. The modeling of the water–metal and organics–metal systems (such as water, benzene, phenol, aminoacids on the Pt (1 1 1), Au (1 1 1), Ni (1 1 1), etc. surfaces) demonstrates that the above mentioned force fields satisfactory describe the surface–organic and surface–water interactions, including the behavior of the interfaces as well (for some examples we refer the readers to [22–33]).

2.2. Metal potential

DL_POLY_2 includes density-dependent potentials suitable for calculating the properties of metals. One of the potentials used in

our MD simulation is the one described by Sutton and Chen (SC or st-ch) [34]:

$$U = \sum_i U_i, \quad (11)$$

$$U_i = \varepsilon \left[\frac{1}{2} \sum_{j \neq i} \left(\frac{a}{r_{ij}} \right)^n - c \sqrt{\rho_i} \right]. \quad (12)$$

Here ρ_i is a density-like term for atom i :

$$\rho_i = \sum_{j \neq i} \left(\frac{a}{r_{ij}} \right)^m. \quad (13)$$

Here the potential has three dimensionless parameters adjustable for the material. They are c , n , and m , and can be chosen for various materials, especially metals. The variable ε sets the energy scale; a is the lattice constant. Table 4 contains the SC potential parameters used for Pt surface.

2.3. Metal surface

The metallic substrate used was cubic Pt, which has the formula Pt₄; in this case we have four atoms for one unit cell in the face-centered-cubic structure and (1 1 1) surface. Pt (1 1 1) surface was arranged in six layers numbering a total of 2352 atoms. The surface area was 60.38 Å²; and the lattice constant was $a = 3.923$ Å. All the parameters of platinum were taken from EIM databases and datasets website supported by the Russian Foundation for Basic Research [35]. Our Pt (1 1 1) surface has the characteristics described by us $z = 4$ and symmetry Fm3 m [36].

3. Results and discussion

Fig. 1 shows a snapshot for an equilibrated state of a water–ethanol–Pt (1 1 1) system with a total of $N = 2954$ molecules; two ethanol and two water molecules are shown separately.

From the MD simulation results, we first estimated the self-diffusion coefficient D for both ethanol and water molecules. We measured D in the absence and presence of a Pt surface. The diffusion coefficient D was estimated for a 50:50% ethanol–water solution at 298 K in the absence of Pt (1 1 1), and the results were compared with those of experimental [9] and other MD

Table 2

Intermolecular Lennard–Jones parameters for ethanol, water, and the Pt (1 1 1) surface.

Group	ε/k (kcal mol ⁻¹)	σ (Å)
C–C	0.12	3.30
C–H	0.00	2.54
C ₁ –Oe	0.16	3.08
H–H	0.00	1.78
H–O	0.00	2.32
Oe–Oe	0.20	2.85
C–Pt	0.94	2.90
Oe–Pt	0.92	2.70
C–OW	0.14	3.43
Oe–OW	0.18	3.20
OW–OW	0.22	3.17

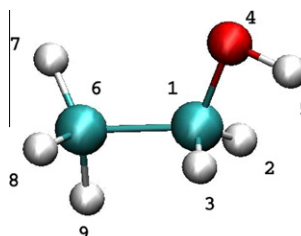
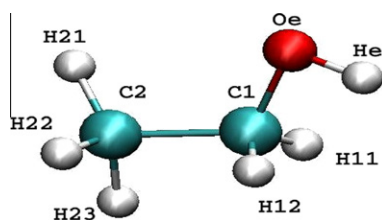


Table 3
The potential parameters used for ethanol molecules.

Bond	Harmonic bond potential = $K(r_{ij} - r_0)^2/2$	
	K (kcal mol ⁻¹ Å)	r_0 (Å)
C ₁ -C ₂	222	1.52
C-H	309	1.11
C ₁ -Oe	428	1.42
Oe-He	545	0.94
Group	Angular potential = $K(\theta_{ijk} - \theta_0)^2/2$	
	K (kcal mol ⁻¹ rad ⁻²)	θ_0 (°)
H ₁ -C ₁ -Oe	45.90	109.44
H ₁ -C ₁ -C ₂	34.60	109.46
H ₁ -C ₁ -H ₁	35.50	120.00
Oe-C ₁ -C ₂	75.70	109.00
He-Oe-C ₁	57.50	109.50
H ₂ -C ₂ -H ₂	35.50	109.50
H ₂ -C ₂ -C ₁	34.60	109.46
Group	Dihedral potential = $K(\phi_{ijkn} - \phi_0)^2/2$	
	K (kcal mol ⁻¹)	ϕ_0 (°)
C ₂ -C ₁ -Oe-He	1.30	180
H ₁₂ -C ₁ -Oe-He	0.14	60
H ₁₁ -C ₁ -Oe-He	0.14	-60
Oe-C ₁ -C ₂ -H ₂₁	0.16	180
Oe-C ₁ -C ₂ -H ₂₂	0.16	60
Oe-C ₁ -C ₂ -H ₂₃	0.16	-60
H ₁₁ -C ₁ -C ₂ -H ₂₁	0.16	-60
H ₁₁ -C ₁ -C ₂ -H ₂₂	0.16	180
H ₁₁ -C ₁ -C ₂ -H ₂₃	0.16	60
H ₁₂ -C ₁ -C ₂ -H ₂₁	0.16	60
H ₁₂ -C ₁ -C ₂ -H ₂₂	0.16	-60
H ₁₃ -C ₁ -C ₂ -H ₂₃	0.16	-180

Table 4
The Sutton–Chen (st–ch) potential parameters of platinum.

ϵ (kcal mol ⁻¹)	a (Å)	N	M	c
0.226	3.92	11.0	7.0	71.336

simulations [37,38]. The diffusion coefficient of ethanol molecules D_e derived from [37] was ranged from 0.98 to $1.0 \times 10^{-9} \text{ m}^2 \text{ s}^{-1}$. The experimental D_e , at the same conditions as in our simulations, was $0.7 \times 10^{-9} \text{ m}^2 \text{ s}^{-1}$; from our simulation, we have obtained D_e to be $0.65 \times 10^{-9} \text{ m}^2 \text{ s}^{-1}$, which is in agreement with experimental results with accuracy of 7.4%. At the same time, the self-diffusion coefficient of water D_w is $1.5 \times 10^{-9} \text{ m}^2 \text{ s}^{-1}$, which is in good agreement with the results of [38], but it is still higher than the experimental one: $0.88 \times 10^{-9} \text{ m}^2 \text{ s}^{-1}$ [9].

Concerning the presence of the Pt (1 1 1) surface, no data are available in the literature; apparently, there has been neither simulation nor experimental research. In our MD simulations, the diffusion coefficients, D_e and D_w , of both water and ethanol are increased in comparison with the results obtained in the absence of the Pt (1 1 1) surface. D_e reaches $1.07 \times 10^{-9} \text{ m}^2 \text{ s}^{-1}$ and D_w reaches $2.1 \times 10^{-9} \text{ m}^2 \text{ s}^{-1}$, which indicates that the presence of the Pt (1 1 1) surface essentially influences the mobility of the ethanol and water molecules. The ethanol and water molecules form an adsorption layer on the Pt (1 1 1) surface. So, we observe competition between the adsorption and diffusion processes while molecules reach the metal surface; the surface and bulk molecules behave differently. It is worth to mention that our model deals with 50:50 ethanol–water systems and it is well known that the diffusion coefficient of the water–ethanol mixture depends on their composition [39].

Next, in Fig. 2 we present the self-diffusion coefficients for water (a) and ethanol (b). The temperature of the system was varied and the temperature effect on the self-diffusion coefficient

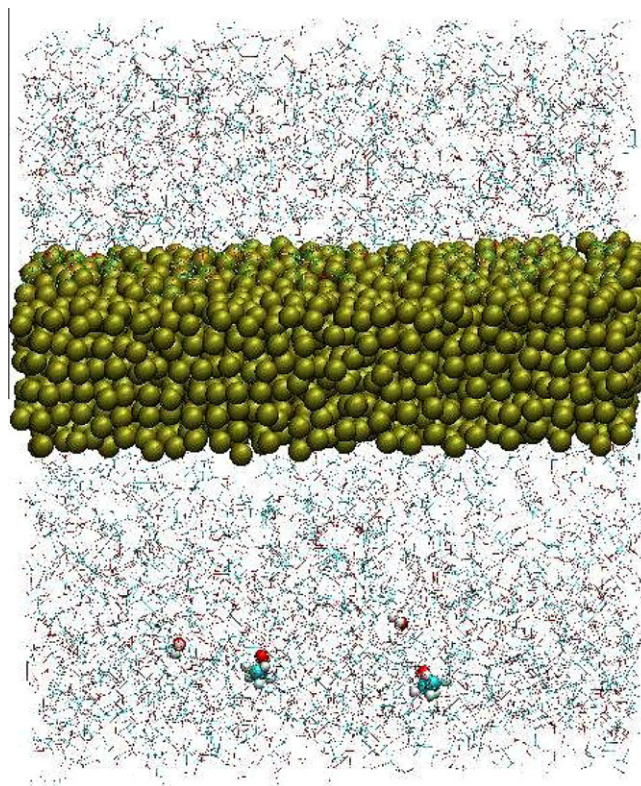


Fig. 1. Snapshot of an ethanol–water–Pt (1 1 1) system at 298 K which consists of 1152 ethanol, 1152 water, and 588 Pt₄ molecules containing a total of 16,176 atoms in a volume $V = (54.92, 54.92, 63.801) \text{ \AA}^3$. The Pt surface shown in the figure seems to be that of an amorphous solid as the thermal vibrations will slightly displace the Pt atoms from their mean equilibrium positions.

for both water and ethanol molecules were investigated. It is shown that the diffusion coefficients decrease with decreasing temperature, which is consistent with the formation of longer H-bonded chains at low temperatures. Initially, at a low temperature (250 K), the presence of the Pt (1 1 1) surface had no effect on the value of D for both water and ethanol. After that, the role of Pt (1 1 1) appears, and the enhancement of the D value in the presence of the Pt (1 1 1) surface is clearly observed, which is consistent with Pt being a good catalyst for such molecules.

It is believed that the self-diffusion coefficient follows an Arrhenius-like relation with temperature [40]. The relationship is

$$D = D_0 \exp(-E/RT).$$

As seen from Fig. 3, the diffusion coefficient of both water and ethanol in the presence of a Pt (1 1 1) obeys the Arrhenius equation; the calculated apparent activation energies (E) of diffusion are 2.5 and 2.91 kcal/mol for ethanol and water, respectively. These low E values explain the higher self-diffusion coefficients of both ethanol and water.

3.1. Intermolecular structure

The structure of liquids is ordinarily expressed in terms of the radial distribution functions (RDF) $g(r)$. The most structured and interesting $g(r)$ functions for liquid ethanol correspond to the O–H and O–O bonding. Fig. 4a and b show the OW–HW and Oe–He RDF graphs of 50:50 ethanol–water mixtures. It is shown that the presence of Pt (1 1 1) does not affect the position of the RDF peaks. However, the inclusion of the Pt (1 1 1) surface notably affects the RDF amplitudes; the first peak at around 2 Å is a strong

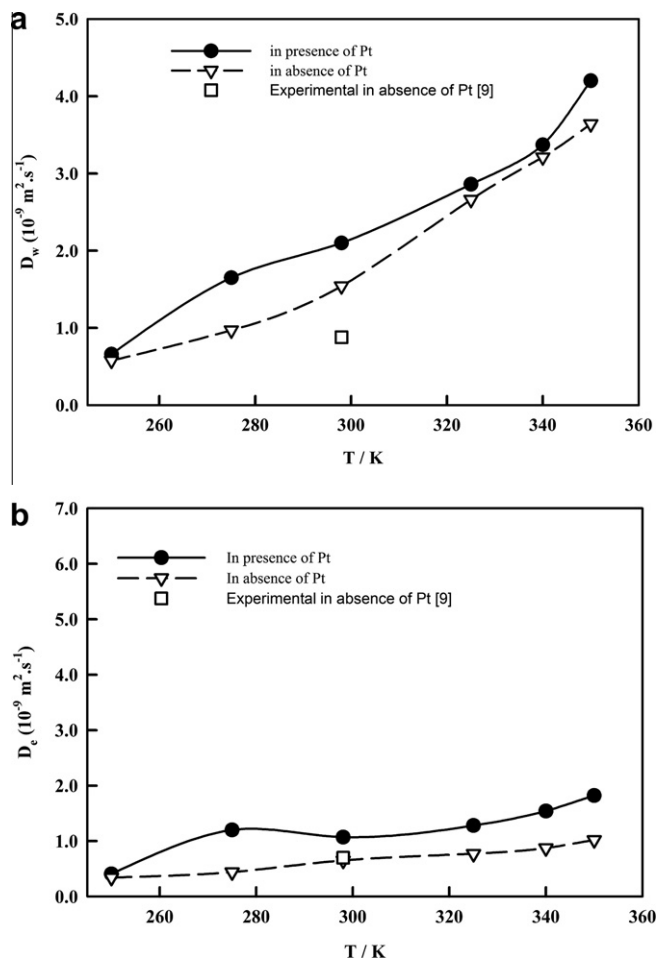


Fig. 2. A temperature dependence of the diffusion coefficient for water (a) and ethanol (b). The solid line represents an ethanol–water–Pt system in the presence of the Pt (1 1 1) surface; the dashed lines represent an ethanol–water system in the absence of a Pt surface.

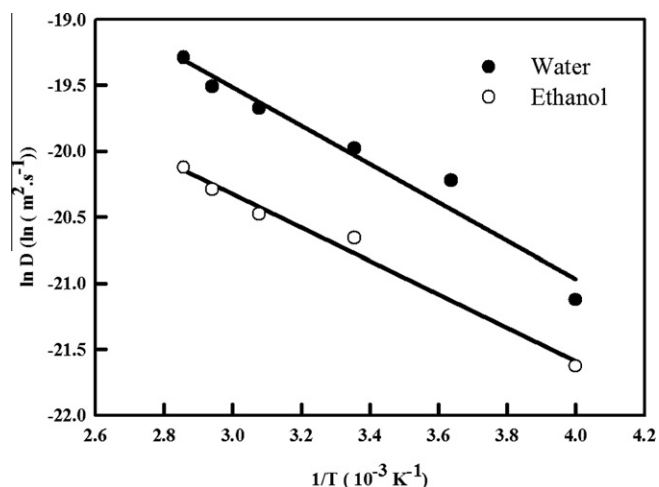


Fig. 3. A temperature dependence of the diffusion coefficient for water and ethanol in presence of a Pt (1 1 1) surface as relation between $\ln D$ and reciprocal of temperature in Kelvin.

evidence of hydrogen bonding in the bulk solution. Fig. 5a and b represent the RDF graphs for Oe–HW and OW–He atomic pairs. It is clear that the Pt (1 1 1) surface enhances the value of $g(r)$,

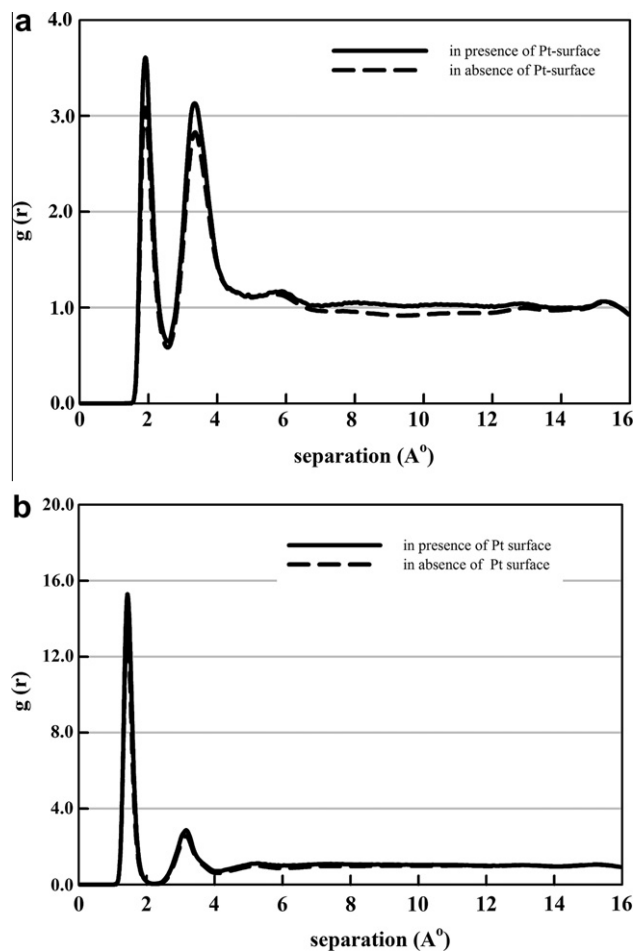


Fig. 4. The radial distribution functions (RDF) of 50:50 ethanol–water mixtures for OW–HW (a) and Oe–He (b). The solid line indicates the presence of the Pt (1 1 1) surface; the dashed line corresponds to the absence of a Pt (1 1 1).

thereby making it easier for ethanol and water to approach each other and to establish a strong interaction between them. Such a strong ethanol–water interaction results in a more preferred ethanol–water structure formation.

In Fig. 6 we present two more RDF graphs for (a) Pt–He and (b) Pt–Oe atomic pair interactions to enlighten a microscopic nature of the water–Pt and ethanol–Pt interactions. More specifically, is hydrogen or oxygen having the higher affinity for Pt (the carbon atoms of ethanol are shielded by the Hs and hence they cannot directly come into contact with the Pt atoms). From the RDF graphs (Pt–He and Pt–Oe) we can guess that the oxygen is present nearer to the surface of Pt (1 1 1) more than H and it is known that both H and O have high affinity toward Pt (1 1 1) surface. This effect is insignificantly small as within the ethanol molecule atoms of two types (Oe and He) are bound rigidly. The estimation of the density profiles as a function of distance from the surface yield similar results for ethanol’s oxygen and hydrogen as shown in Fig. 7.

In addition to Figs. 4–6, we have built new graphs (Fig. 5C in supporting information) to compare the behavior of the RDF for oxygen and hydrogen in water and in ethanol when the molecules are in the adsorption layer and when they are in the bulk solvent. The RDF of Fig. 5C for OW–He (a) and Oe–HW (b) have shown the atomic pairs rearrangement at the earlier stages of the dynamics (when the ethanol–water solvent over the Pt (1 1 1) surface is yet forming a well-mixture bulk) and at the later final states (when mostly ethanol molecules lie on the Pt (1 1 1) surface forming a well-distinguished adsorption layer). The behaviors of RDF in

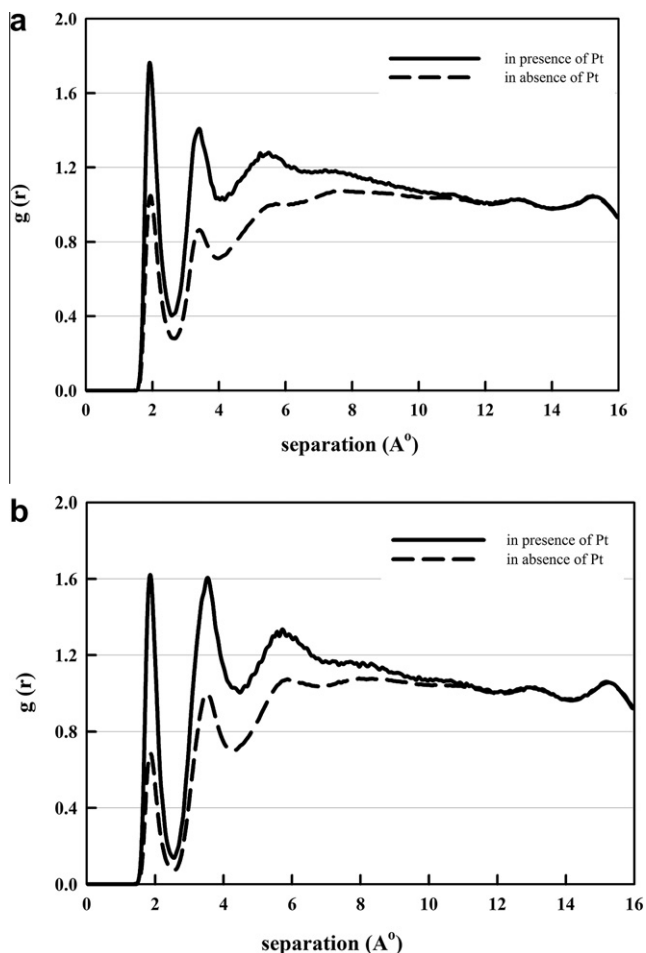


Fig. 5. The radial distribution functions (RDF) of 50:50 ethanol–water mixtures for Oe–HW (a) and OW–He (b). The solid line indicates the presence of a platinum surface; the dashed line corresponds to the absence of a platinum surface.

Fig. 5C indicate that the formation of an adsorption layer lowers the atomic pair structural ordering between the ethanol and water molecules. Additionally generated animation movies have also shown that during the adsorption process on the Pt (1 1 1) surface the ethanol molecules push water molecules from the surface toward the bulk phase. The comparison of the RDF in Fig. 5C (a) and (b) are straightforward.

3.2. Density profiles

In Fig. 7, the density profiles of both ethanol and water are plotted versus the distance from the surface where the densities are normalized relative to the density of the bulk solution. The results show that the density of ethanol molecules in the first layer is higher than that of water molecules. But for the second layer it is different. From this result, we can suggest that hydrogen networks between water and ethanol are disrupted as the solution mixture approaches the Pt (1 1 1) surface. At a large distance from the surface, the relative density of the liquids – ethanol and water – approaches unity as it would be expected in a bulk environment with no electrode influence. The results also imply that ethanol molecules push the water molecules away from the surface thereby forming a strongly adsorbed layer on the Pt (1 1 1) surface.

It is known that the diffusion coefficient of pure water or ethanol is larger than that of the 50:50 liquid. From the density profile illustrated above, the density of ethanol molecules on the first

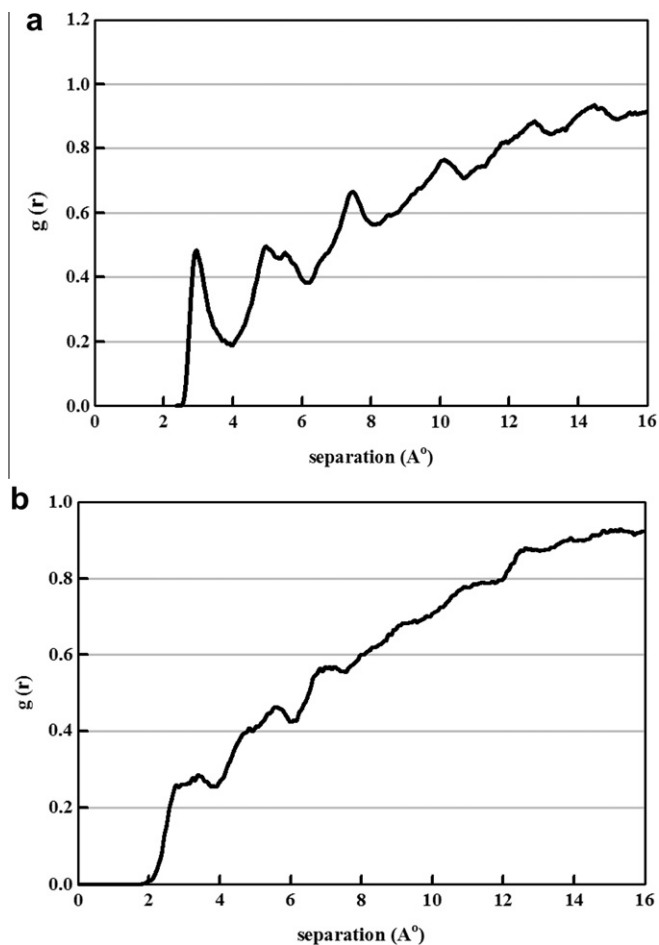


Fig. 6. The radial distribution functions (RDF) of 50:50 of the ethanol–water mixture interactions with surface for Pt–He (a) and Pt–Oe (b).

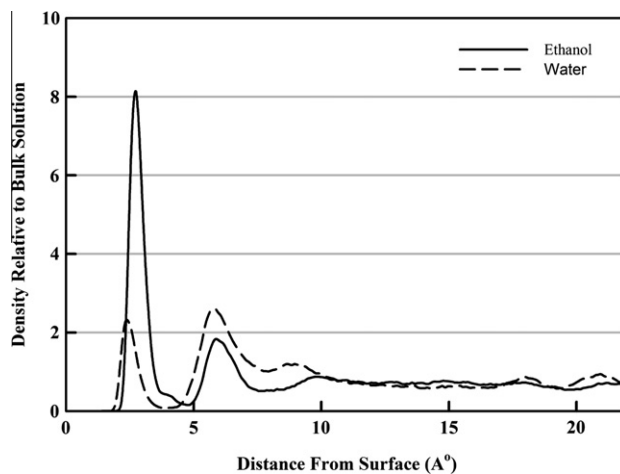


Fig. 7. The density profile of an ethanol–water system in the presence of Pt (1 1 1) surface. The densities of both ethanol and water were normalized relative to the bulk density of the solution, which is 0.8 g/cm³.

layer is higher than that of water molecules. But for the second layer it is different; the law is opposite. From this we can suggest that the hydrogen networks between water and ethanol are disrupted; then near the surface the liquid mixture is more like either water or ethanol. The diffusion coefficient will become larger. For the RDF its amplitude in the case of 50:50 is larger. Thus,

water–water or ethanol–ethanol molecule interaction will intensify, thereby governing the total system's dynamics.

It should be noted that all of the results presented above are constructed for a bulk solution, and they are not related specifically to the adsorbed molecules; the same interpretations are true for the $g(r)$ graphs. (It is well known that the 2D surface diffusion is different from that of a bulk solution.) From our MD simulations, the diffusion coefficient is higher in the presence of a Pt (1 1 1) than in its absence. Apparently, as experimental and theoretical results indicate, the diffusion coefficient is always higher in the presence of many active metallic surfaces than in their absence. We observe a similar regularity in the presence of a Pt (1 1 1). This is because the Pt (1 1 1) surface is a good catalyst of ethanol oxidation or dissociative adsorption. Such adsorption process makes the bulk of ethanol to adsorb on the surface, so it actively increases the mobility of the solution molecules toward the surface. In this aspect, a good correlation of our MD simulation results with experimental observations is clear. It is likely, however, that an interface and a bulk solvent have different properties, and more detailed correlation between the RDF function and diffusion coefficient could clear up other aspects of the atomistic simulation. For example, dividing the properties such as the diffusion coefficient and MD trajectory into separate dimensions and reporting how diffusion changes as a function of distance from the surface looks reasonably straightforward, which would demonstrate more new phenomena for possible experiment realization.

4. Conclusion remarks

We simulated a water–ethanol mixture in the presence and absence of the Pt (1 1 1) surface using DL_POLY code (version 2.19). The self-diffusion coefficients of both water and ethanol in the presence and absence of the Pt (1 1 1) surface were calculated; an excellent agreement with the experimental results has been found within an error of 7.4%. The enhancement of the self-diffusion coefficients of both water and ethanol molecules related to the ethanol–water structure have been well established in the presence of a Pt (1 1 1). The radial distribution functions (RDF) graphs have been built, and RDF correlations with the self-diffusion coefficients of both ethanol and water molecules are also illustrated. It is shown that the presence of Pt (1 1 1) does not affect the position of the RDF peaks. However, the inclusion of the Pt (1 1 1) surface notably affects the RDF amplitudes; the first peak at 2 Å is a strong evidence of hydrogen bonding in the bulk solution. The RDF graphs for Oe–HW and OW–He atomic pairs demonstrate that the Pt (1 1 1) surface enhances the value of $g(r)$, thereby making it easier for ethanol and water to approach each other and to establish a strong interaction between them. Such a strong ethanol–water interaction results in a more preferred ethanol–water structure formation.

Acknowledgement

This work has been performed in the framework of joint collaborative agreement Arab Republic of Egypt (ARE) – Joint Institute for Nuclear Research (JINR) (Project #302). This work was supported in part by the Grant in Aid for the Global Center of Excellence Program of the Center for Education and Research of Symbiotic, Safe and Secure System Design from Japan's Ministry of Education, Culture, Sport, and Technology. The MD simulations have been performed using computer software, hardware facilities, and cluster

machines at the CICC (JINR), RICC (RIKEN), and Yasuoka Laboratory of Keio University (Japan). We thank Prof. Vladimir Korenkov (LIT, JINR) for providing us with computer time at CICC, and Prof. Evgeny Krasavin (LRB, JINR) for his encouraging support. The authors would like to specially thank Mr. Sergei Negovellov (JINR) for technical assistance and helpful comments.

References

- [1] C.A. Cardona, O.J. Sánchez, *Biores. Technol.* 98 (2007) 2415.
- [2] O.J. Sánchez, C.A. Cardona, *Biores. Technol.* 99 (2008) 5270.
- [3] S.Y. Shen, T.S. Zhao, J.B. Xu, *Int. J. Hydrogen Energy* 35 (2010) 12911.
- [4] V.N. Vasudevan, M.V. Leland, *J. Membr. Sci.* 306 (2007) 209.
- [5] S.Q. Song, P. Tsiakaras, *Appl. Catal. B* 63 (2006) 187.
- [6] S.Q. Song, W.J. Zhou, Z.H. Zhou, L.H. Jiang, G.Q. Sun, Q. Xin, V. Leontidis, S. Kontou, P. Tsiakaras, *Int. J. Hydrogen Energy* 30 (2005) 995.
- [7] W. Yao-Chun, C. Chuan, J.U. Shin-Pon, *Chin. J. Catal.* 29 (2008) 1099–1106.
- [8] T. Kousksou, A. Jamil, Y. Zeraouli, J.P. Dumas, *Chem. Eng. Sci.* 62 (2007) 6516.
- [9] C. Zhang, X. Yang, *Fluid Phase Equilib.* 231 (2005) 1.
- [10] P.G. Kusalik, A.P. Lyubartsev, D.L. Bergman, A. Laaksonen, *J. Phys. Chem. B* 104 (2000) 9533.
- [11] A.K. Soper, J.L. Finney, *Phys. Rev. Lett.* 71 (1993) 4346.
- [12] W.M.H. Sachtler, M. Ichikawa, *J. Phys. Chem.* 90 (1986) 4758.
- [13] A. Galal, N.F. Atta, S.A. Darwish, S.M. Ali, *Top Catal.* 47 (2008) 73.
- [14] Kh. Kholmurodov, I. Puzynin, W. Smith, K. Yasuoka, T. Ebisuzaki, *Comput. Phys. Commun.* 141 (2001) 1.
- [15] C.Y. David, *Computational Chemistry: A Practical Guide for Applying Techniques to Real-World Problems*, John Wiley & Sons, Inc., New York, 2001.
- [16] K. Miyabe, S. Takeuchi, *Can. J. Chem. Eng.* 76 (1998) 887.
- [17] D.J. Cooke, R.J. Gray, K.K. Sand, S.L.S. Stip, J.A. Elliott, *Langmuir* 26 (2010) 14520.
- [18] W. Smith, T.R. Forester, *J. Mol. Graph.* 14 (1996) 136.
- [19] W. Smith, T.R. Forester, I.T. Todorov, *THE DL POLY 2 USER MANUAL*, STFC Daresbury Laboratory Daresbury, Warrington WA4 4AD Cheshire, UK, Version 2.19, April 2008.
- [20] B.R. Brooks, C.L. Brooks III, A.D. Mackerell, L. Nilsson, R.J. Petrella, B. Roux, Y. Won, G. Archontis, C. Bartels, S. Boresch, A. Caffisch, L. Caves, Q. Cui, A.R. Dinner, M. Feig, S. Fischer, J. Gao, M. Hodoscek, W. Im, K. Kuczera, T. Lazaridis, J. Ma, V. Ovchinnikov, E. Paci, R.W. Pastor, C.B. Post, J.Z. Pu, M. Schaefer, B. Tidor, R.M. Venable, H.L. Woodcock, X. Wu, W. Yang, D.M. York, M. Karplus, *CHARMM: The Biomolecular simulation Program*, *J. Comp. Chem.* 30 (2009) 1545–1615.
- [21] CHARMM c36b1 Documentation. HTML formatting scripts developed by R.M. Venable, NIH/NHLBI/DIR, Lab. of Comput. Bio. <http://www.charmm.org/documentation/c36b1/index.html>.
- [22] P. Bjelkmar, P. Larsson, M.A. Cuendet, B. Hess, E. Lindahl, *J. Chem. Theory Comput.* 6 (2010) 459.
- [23] N.F.A. van der Vegt, W.F. van Gunsteren, *J. Phys. Chem. B* 108 (2004) 1056.
- [24] P. Schravendijk, N. van der Vegt, *J. Chem. Theory Comp.* 1 (2005) 643.
- [25] S. Patel, Ch.L. Brooks, *J. Chem. Phys.* 123 (2005) 164502.
- [26] T.M. Glennon, Y.-J. Zheng, S.M. Le Grand, B.A. Shutzberg, K.M. Merz Jr., *J. Comput. Chem.* 15 (9) (1994) 1019–1040.
- [27] T.E. Cheatham III, M.F. Crowley, T. Fox, P.A. Kollman, *Proc. Natl. Acad. Sci.* 94 (1997) 9626.
- [28] X. Xia, L. Perera, U. Essmann, M.L. Berkowitz, *Surf. Sci.* 335 (1995) 401.
- [29] V.M. Anisimov, I.V. Vorobyov, B. Roux, A.D. Mackerell Jr., *J. Chem. Theory Comput.* 3 (6) (2007) 1927, <http://dx.doi.org/10.1021/ct700100a>.
- [30] J.I. Siepmann, M. Sprick, *J. Chem. Phys.* 102 (1995) 511.
- [31] H. Sakuma, T. Tsuchiya, K. Kawamura, K. Otsuki, *Surf. Sci.* 536 (2003) L396.
- [32] A. Michaelides, V.A. Ranea, P.L. de Andres, D.A. King, *Phys. Rev. Lett.* 90 (21) (2003) 216102.
- [33] C. Morin, D. Simon, P. Sautet, *J. Phys. Chem. B* 108 (2004) 5653.
- [34] A.P. Sutton, J. Chen, *Philos. Mag. Lett.* 61 (1990) 139.
- [35] WWW-MINCRYST, Crystallographic and Crystallochemical Database for Minerals and their Structural Analogues. <http://database.iem.ac.ru/mincryst/>.
- [36] (1) C. Palache, H. Berman, C. Frondel, *Dana's system of mineralogy*, 7th ed., vol. 1, 1944, pp. 106–109. (2) L.J. Cabri, C.E. Feather, *Platinum–iron alloys; nomenclature based on a study of natural and synthetic alloys*, *Can. Mineral.* 13 (1975) 117–126. (3) D.C. Harris, L.J. Cabri, *Nomenclature of platinum-group element alloys: review and revision*, *Can. Mineral.* 29 (1991) 231–237. (4) NBS Circ. 539, 1, 31. (5) A.J. Criddle, C.J. Stanley (Eds.), *Quantitative data file for ore minerals*, 3rd ed., Chapman & Hall, London, 1993, p. 441.
- [37] S.P. William, I. Hiroyuki, A. Yoji, *J. Phys. Chem. A* 107 (2003) 4784.
- [38] E.J.W. Wenisik, A.C. Hoffmann, P.J. Van Maaren, D. Van der Spoel, *J. Chem. Phys.* 119 (2003) 7308.
- [39] C. Zhang et al., *J. Chem. Phys.* 125 (2006) 104502.
- [40] W. Li, C. Chen, J. Yang, *Heat Tran. Asian Res.* 37 (2008) 86.